Enhanced Piezoelectric Effect Derived from Grain Boundary in MoS_2 Monolayers

Mingjin Dai,[†,‡,#] Wei Zheng,[†,‡,&,#] Xi Zhang,[*,§] Sanmei Wang,[§] Junhao Lin,[‖] Kai Li,[¶] Yunxia Hu,[†,‡] Enwei Sun,[¶] Jia Zhang,[‡] Yunfeng Qiu,[‡] Yongqing Fu,[⊥] Wenwu Cao,[¶] and PingAn Hu[*,†,‡,Φ]

[†]School of Materials Science and Engineering, Harbin Institute of Technology, Harbin 150001, P.R. China

[‡]MOE Key Laboratory of Micro-Systems and Micro-Structures Manufacturing, Harbin Institute of Technology, Harbin 150001, P.R. China

[§]Institute of Nanosurface Science and Engineering & Guangdong Provincial Key Laboratory of Micro/Nano Optomechatronics Engineering, Shenzhen University, Shenzhen 518060, P.R. China

[‖]Department of Physics, Southern University of Science and Technology, Shenzhen 518055, P.R. China

[¶]School of Instrument Science and Engineering, Harbin Institute of Technology, Harbin 150080, P.R. China

[⊥]Faculty of Engineering & Environment, Northumbria University, Newcastle upon Tyne, NE1 8ST, United Kingdom

[Φ]Institute for Advanced Ceramics, Harbin Institute of Technology, Harbin 150001, P.R. China

[&]College of Physics, Qingdao University, Qingdao 266071, P.R. China

Abstract: Recent discovery of piezoelectricity existed in two-dimensional (2D) layered materials represents a key milestone for flexible electronics, miniaturized and wearable devices. However, the so far reported piezoelectricity in these 2D layered materials is too weak to be used for any practical applications. In this work, we discovered that grain boundaries (GBs) in monolayer MoS_2 can significantly enhance its piezoelectric property. The output power of piezoelectric devices made of the butterfly-shaped monolayer MoS_2 was improved about 50% by the GB induced piezoelectric effect. The enhanced piezoelectricity is attributed to the additional piezoelectric effect induced by the existence of deformable GBs which can promote polarization and generates spontaneous polarization with different piezoelectric coefficients along with various directions. We further made a flexible piezoelectric device based on the 2D MoS_2 with the GBs and demonstrated its potential application in self-powered precision sensors for *in-situ* detecting pressure changes in human blood for the health monitoring.

Keywords: SHG, AC-STEM, DFT calculations, piezoelectric sensors, health monitoring

Introduction

Piezoelectric materials can generate electric charges in proportion to the externally applied stress, and vice versa. Therefore, they can realize the conversion between electrical and mechanical energy.[1,2] Traditionally, piezoelectricity can be observed in crystalline materials lacking the inversion symmetry.[1,3] Various forms of piezoelectric materials, such as bulk crystals, thin films, and nanowires, have been extensively studied and widely used for applications in sensors, actuators, transducers and energy harvesters.[4, 5] Very recently, two-dimensional (2D) materials have been reported to be piezoelectrics.[6-9] Compared with the conventional piezoelectric materials, 2D layered piezoelectric materials have higher crystal quality and can withstand much larger elastic strains,[10-12] which makes them suitable for transparent and flexible self-powered electronic switches, skins and sensors.[13-16]

Monolayer crystalline materials, such as hexagonal boron nitride (*h*-BN) and transition metal dichalcogenides (TMDs), could lose their center-symmetry (which commonly exists in their corresponding bulk counterparts), and exhibit piezoelectric properties.[17,18] The coefficients of piezoelectric strain (d_{11}) and piezoelectric stress (e_{11}) of the 2H-TMD monolayers are comparable to, sometimes even better than, those of the conventional bulk piezoelectric materials, such as AlN and GaN.[3] Duerloo et

al. theoretically predicted the existence of piezoelectricity in monolayers of BN, MoS_2, $MoSe_2$, $MoTe_2$, WS_2, WSe_2, and WTe_2.[19] Wang et al studied the piezoelectricity of monolayer MoS_2 for applications in energy conversion and piezotronic devices.[6] They discovered that ultrathin MoS_2 with odd-layers could produce oscillating piezoelectric voltage and current outputs, whereas no piezoelectric output was observed for the MoS_2 with even-layers. Following these pioneering works, extensive studies have been conducted recently to understand the piezoelectric properties of various ultrathin 2D materials and explore new types of monolayer materials with higher piezoelectricity.[7,20-24] For example, Kim et al. reported orientation-dependent piezoelectricity in the monolayer MoS_2 grown by chemical vapor deposition (CVD), and the output power obtained from the armchair direction of MoS_2 was found about twice as much as that from the zigzag direction under the same strain.[20] Zhu et al. used atomic force microscopy (AFM)-based method to investigate the piezoelectric effect in the devices made of triangle monolayer MoS_2 and their results showed that the conductivity of MoS_2 can be actively modulated by the electric field induced by piezoelectric charged polarization at different strains.[7] Li et al. also theoretically predicted intrinsic piezoelectric effects in monolayers of group-III (MX, M=Ga or In, X=S or Se) and group IV monochalcogenides (MX, M=Sn or Ge, X=Se or S) with large piezoelectric coefficients.[24]

In the case of practical applications, large-scale monolayer 2D piezoelectrics are needed. However, for large-scale CVD-grown 2D materials, there are many grains and grain boundaries (GBs), which are interfaces among adjacent grains with different crystalline orientations.[25-27] The GBs in the monolayer MoS_2 can be described as an array of diverse dislocation cores formed by sulfur substituted 4-6, 4-8, 5-7, and 6-8 Mo-S rings, which have recently been identified using transmission electron microscopy (TEM).[25-30] These GBs can significantly influence mechanical, optical and electrical properties of the MoS_2.[31-33] Therefore, the influences of GBs on the piezoelectric properties of 2D materials, such as MoS_2 monolayers, are needed to be explored.

Here, we studied the atomic structure of GBs in monolayer MoS_2 flakes and supposed the enhanced piezoelectric effect induced by the existence of deformable GBs. First principle calculations and the piezoelectric force microscopy (PFM) measurements provided sufficient evidence for the GB enhancement of piezoelectric behavior. In addition, the piezoelectric power output of MoS_2 with grain boundaries (GB-MoS_2) is 50% higher than that of MoS_2 single crystal (SC-MoS_2). This discovery allows us to apply the butterfly-shaped GB-MoS_2 to self-powered force sensors, illustrating its great potential in the application of flexible/wearable devices.

Results and discussion

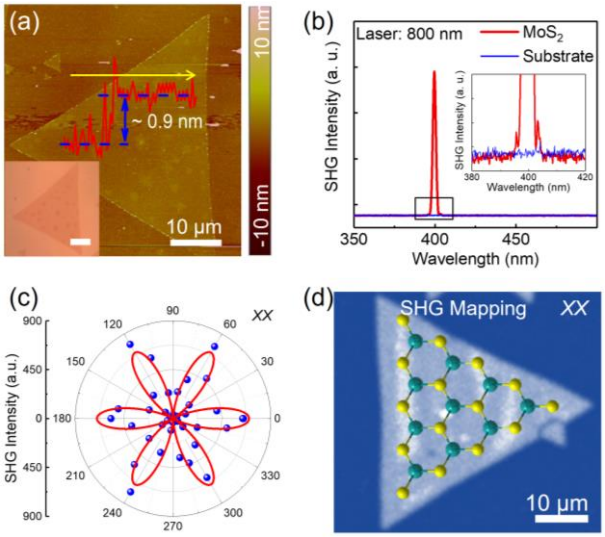

Figure 1. Characterization of single-crystalline monolayer MoS_2 flakes. (a) The AFM image of triangle monolayer MoS_2 flake. Inset: the corresponding optical image. Scale bars: 10 μm. (b) SHG spectrum obtained both from MoS_2 flake and substrate. (c) The polarization angle θ dependent SHG intensity under parallel conditions (*XX*). It exhibits a clear six-fold rotational symmetry ($I = I_0 \cos^2(3\theta)$). (d) SHG mapping of a triangle MoS_2 flake on SiO_2/Si substrate.

Structure Characterizations of SC- and GB-MoS_2 Monolayers. In our experiments, MoS_2 flakes were synthesized on SiO_2/Si substrate using a CVD method with the precursors of molybdenum trioxide (MoO_3) and sulfur (S).[15] The thickness of monolayer MoS_2 was identified using an atomic force microscopic (AFM). As shown in Figure 1a, the monolayer MoS_2 flake with triangle shape has a thickness of ~ 1 nm. As reported, when the thickness of MoS_2 is a monolayer, the structure becomes noncentrosymmetric.[6] Optical second harmonic generation (SHG) microscopy is a powerful tool for determining the crystallographic orientation and visualizing GB structures of the as-grown CVD MoS_2. Additionally, the SHG is highly sensitive to structural symmetry, therefore, it can be used to identify the armchair or zigzag directions of monolayer MoS_2 through analysis of the anisotropic polarization patterns.[34] In order to investigate the noncentrosymmetric crystal structure, SHG measurements were carried out. As shown in Figure 1b, a clear SHG peak for monolayer MoS_2 flake is located at 400 nm when an 800 nm laser was used as the excitation light source, while no signal for the bare substrate. This indicates the noncentrosymmetric structure of monolayer MoS_2 flakes.[9,34] Furthermore, the angle dependence of SHG intensity taken in parallel (*XX*) or vertical (*XY*) polarization configurations shows a 6-fold rotational symmetry ($I=I_0 \cos^2(3\theta)$), which also validates that the monolayer MoS_2 possesses

a 3-fold rotational symmetry (Figure 1c and Figure S1 in Supporting Information). And it can be confirmed that the armchair direction is perpendicular to the edge according to the SHG patterns.[33] In addition, the uniform intensity shown in polarized SHG mapping illustrates the single-crystal characteristic of triangle-like MoS_2 monolayer.

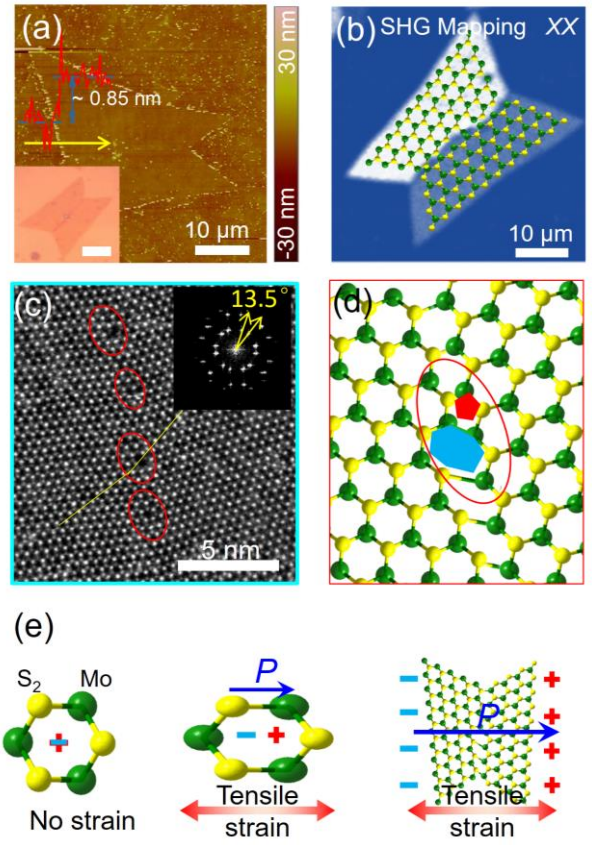

Figure 2. Characterization of GB in monolayer MoS_2 flakes. (a) The AFM image of triangle monolayer MoS_2 flake. Inset: the corresponding optical image. Scale bars: 10 μm. (b) SHG mapping of a butterfly-shaped MoS_2 flake on SiO_2/Si substrate. (c) AC-STEM-ADF image of the GB with a ~13.5° rotation angle. Inset: the corresponding FFT image. (d) The atomic schematic of GB of monolayer MoS_2 flake. (e) The schematic diagram of in-plane polarization under tensile strain in GB-MoS_2 monolayers.

As for the butterfly-shaped monolayer GB-MoS_2 flake, the thickness is extracted from the AFM image indicating its monolayer form (Figure 2a). More importantly, the polarized SHG mapping shown in Figure 2b reveals the GB-MoS_2 indeed consists of two grains and a GB at the interface of them. More SHG mapping results obtained from GB-MoS_2 monolayers are shown in Figure S2. Strong and uniform SHG signal was observed inside the grains. The dark line, which may be caused by defects, indicates the location of the GBs. Subsequently, aberration-corrected scanning transmission electron microscopy (AC-STEM) was used to examine the structure of GBs in the butterfly-shaped monolayer GB-MoS_2 flake (Figure S3). The AC-STEM annular dark-field (ADF) image from a GB with a rotation angle of ~13.5° is shown in Figure 2c, and the inset is the Fourier Transform (FFT) image showing two sets of MoS_2 diffraction spots with a rotation angle of 13.5°. From the high-resolution image shown in Figure 2c and Figure S4, the GB is basically consisted of 5-7 members of rings as the fundamental units, with a lot of other defects along the GBs. As shown in Figure 2d, the GB of the monolayer MoS_2 is formed by two grains which have different crystal orientations and are connected at the GB through chemical covalent bonds. This is very consistent with the results of SHG mapping measurements. Particularly, the strain-induced dipoles of two grains will be not cancelled absolutely due to their crystalline orientations.

Additionally, Raman and photoluminescence (PL) spectra are taken from the SC and GB area, respectively. Figure S5a shows the Raman spectra of E_{2g} and A_{1g} modes of the SC-MoS_2 and GB-MoS_2 with and without a uniaxial (x-axis) strain. The A_{1g} mode of Raman spectra did not show apparent changes for both SC and GB with/without strain. While, under the applied strain, there was an obvious blue-shift for the E_{2g} mode in the monolayer MoS_2 with and without GBs, respectively. It is worth noting that the amplitude change of the E_{2g} mode for the GB-MoS_2 is much larger than that of SC-MoS_2, indicating a larger deformation under the same applied strain. Effects of applied strain on PL responses of MoS_2 with GBs and the MoS_2 without GBs were studied and the results are shown in Figure S5b. An enhancement of the PL intensity is observed in GB-MoS_2 comparing with the SC-MoS_2. The half peak width of the PL spectrum at the GB is much larger than that of places without GB in the same sample. According to previous studies, defects at the GBs may contribute to the increase of half peak width and the amplitude of the PL intensity. [34] When a uniaxial strain (e.g. 0.42% strain in this case) is applied onto the MoS_2, the PL peaks show red-shift observed at the locations SC and GB. The increased red-shift of PL peak (from 20 to 26 meV) at the GB indicates that the PL spectrum at the GB location is more sensitive to the change of uniaxial strain, and there is a change of bandgap structures.

Our observation reveals that the GBs in the monolayer MoS_2 are more complicated than the "periodical" structure as modeled in the theoretical analysis.[26,27] If a tensile strain is applied to GB-MoS_2 monolayers, an enhanced polarization by GB will be generated due to its noncentrosymmetric structure (Figure 2e).

Enhanced Piezoelectric Effect by GB in MoS_2 Monolayers. To further understand the influence of GBs on the structural evolution, dipole moment, and the electronic structures under a tensile strain for the monolayer

MoS_2, first-principle density-functional theory (DFT) calculations were performed using the DMOL^3 package within the general gradient approximation (GGA) expressed by the Perdew-Burke-Ernzerh functional (PBE) and with the double numeric atomic orbital plus polarization basis set.[36,37] In the geometry optimization, the convergence tolerances for the energy, force, and displacement were set to be 10^{-5} Hartree, 0.002 Hartree per Å, and 0.005 Å, respectively. The atomic structures of single-crystalline armchair-edged MoS_2 ribbon and GB-MoS_2 ribbon with uniaxial tensile strains are shown in Figure 3a and b. All dangling bonds are passivated by hydrogen atoms to stabilize the structures. At the edges, a Mo atom is terminated by two H atoms and an S atom is terminated by an H atom.[38] Two MoS_2 grains in Figure 3b are connected by a 7-atom ring and a 5-atom ring denoted as the GBs. The GB unit cell has the element configuration of $Mo_{17}S_{34}H_{13}$. At the boundary, two 3-coordinated Mo atoms form a Mo-Mo bond and were terminated by one bridging H atom. Thus, the Mo-S-Mo-S… chain was interrupted at the GB. A spared Mo atom introduces a hole-impurity into the system. The boundary edge shows a combined the ratio of 1:2 for armchair one and zigzag ratio one. The DFT-derived dipole moments (μ), including μ_y and μ_z components, under a uniaxial tensile strain along the x-axis direction are shown in Figure 3c and d. Compared with the SC ribbon, GB ribbon possesses larger values of μ_y and μ_z. We also performed calculations in the hybrid functional (HSE06) level. Figure S6 shows the Y dipole moment of GB-MoS_2 reaches to ~0.88 Debye, while the Y dipole moment of SC-MoS_2 is lowered to ~0.3 Debye of HSE level. The higher GB/SC ratio of dipole moment of HSE calculation confirmed that the higher piezo-current comes from the GB structure. They are considerably larger and increase with the strain ε. As a result, GB will intensify the piezoelectric effect due to its large dipole moments under the same strain conditions.

Furthermore, we investigated the changes of band structures under a tensile strain using density functional theory (DFT) calculations for both SC ribbons and GB ribbons (Figure S7 and Figure S8). For the SC ribbon, an indirect bandgap (E_G) was obtained from the Γ point to the M point in the Brillouin zone. The indirect bandgap E_G shrinks from 0.437 eV to 0.386 eV when the strain ε increases from 0% to 6% along the x-axis, which is matched well by direct bandgap changing (PL measurements shown in Figure S5). This is because the uniaxial tensile strain increases the separation of the Mo and S along the x-direction and decreases the charge density, thus leading to the suppression of the repulsion interactions between bonding states in the valence band and antibonding states in the conduction band. The decrease of E_G increases the possibility of electron to transport from the valence band to the conduction band, which is not beneficial for piezoelectricity in semiconductors because of the screening effect induced by free carriers. However, for the GB ribbons, the Fermi-level (E_F) shifts down into the valence band. The ribbon shows a p-type conduction behavior since the GBs introduce the interruption of the Mo-S-Mo-S... chain and the Mo-Mo bond formed at the GBs provide hole states. When the tensile strain ε increases from 0% to 6%, the position of E_F increases but the disparity between E_F and the top of the valence band is reduced from 0.19 eV to 0.115 eV. The p-type nature of the GB ribbons provides empty states near the E_F, and assists the strain-induced charges, which can further enhance the piezoelectricity in GB-MoS_2 flakes.

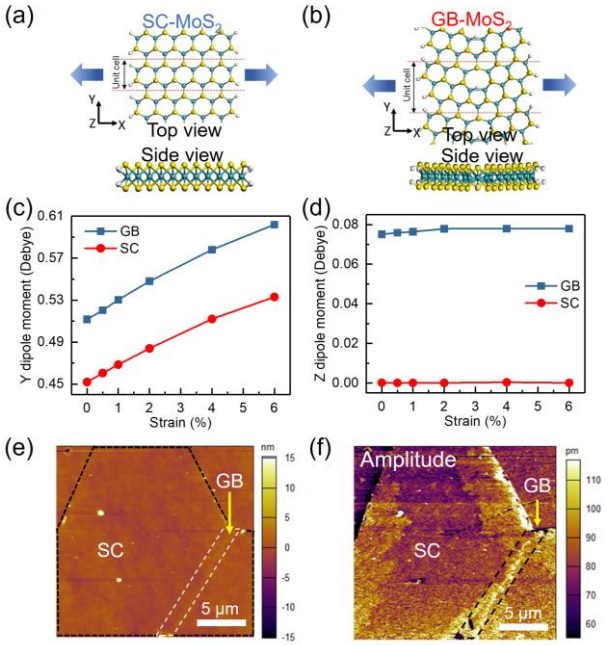

Figure 3. Theoretical and experimental study on the origins for GB enhanced piezoelectricity. (a,b) The model of MoS_2 ribbons terminated with H atoms (white balls) for DFT calculation. Top view of single crystalline (left) and domain boundary (right), and corresponding side view (bottom), respectively. (c,d) The calculated dipole moment of MoS_2 ribbons under a uniaxial tensile strain. (e) The AFM height retrace images of GB in butterfly-shaped monolayer MoS_2 flake. (f) The PFM amplitude images of GB in butterfly-shaped monolayer MoS_2 flake.

PFM measurement is used to characterize the local vertical piezoelectric effect of the samples. Depending on the directions between the applied field and polarization vectors, sample deformation can be elongation, contraction or shear. According to the piezoelectric effect, the field-induced strain S_j can be expressed as equation 1:

$$S_j = d_{ij} E_i \quad (1)$$

where d_{ij} are components of the piezoelectric coefficient tensor (in reduced Voigt notation) and E_i is the applied field. The crystal structure of monolayer MoS_2 belongs to D_{3h} point group.[37] Thus, there is only one non-

zero independent coefficient e_{11}. The in-plane polarization (P_1) along the x-axis can thus be expressed as $P_1 = e_{11}(\varepsilon_{11} - \varepsilon_{22})$. When an electric field or voltage is applied at a certain angle from the vertical direction using the PFM tip, there will be a strain applied to the x-axis onto the MoS_2. Under the same voltage, a stronger deformation will indicate a more significant piezoelectric effect. Figure 3e shows the obtained AFM image of the butterfly-shaped MoS_2 with a GB, and indicates a flat surface with a thickness of ~1 nm. As shown in Figure 3f, the amplitude image of MoS_2 with the GB shows a very different contrast between MoS_2 and the SiO_2 areas, indicating that this is an effective way to study the piezoelectric properties of monolayer MoS_2. On the other hand, the SC area shows a uniform amplitude retrace of ~100 pm. While a larger amplitude (>110 pm) is found at the location of GB-MoS_2, which indicates a larger piezoelectric effect in the z-axis direction. This is consistent with the theoretical result as shown in Figure 3d.

Additional Lateral Piezoelectric Outputs Induced by Grain Boundaries. In order to investigate the piezoelectric outputs in the in-plane of MoS_2 monolayers, two kinds of devices were fabricated. Figure S9 shows a schematic representation of the fabricated two kind devices for measuring the piezoelectric properties. Encapsulation using polydimethylsiloxane (PDMS) can prevent slippage between the material and the electrode during measurements. A schematic drawing for estimating strain in the MoS_2 device is shown in Figure S10. Because the dimensions of MoS_2 flakes are much smaller than those of polyethylene terephthalate (PET) substrates, it can be assumed that the mechanical behaviors of the substrate will not be affected by the MoS_2 flake. The strain induced in the MoS_2 can be estimated using the equation 2:[6]

$$\varepsilon = \pm 3\times(a/2l) \times (D_{max}/l) \times(1-Z_0/l) \quad (2)$$

where a is the thickness of PET (~1 mm), l is the length of PET (~4 cm), D_{max} is the displacement of the free end of the substrate, and Z_0 is the distance between the MoS_2 flakes and the fixed edge (~1 cm). The applied strain was limited to less than 0.8% in order to avoid sample slippage. The piezoelectric response was recorded by applying an external strain to the devices, and the strain-induced polarization charges can drive the flow of the electrons in an external circuit (Figure 4a and d).

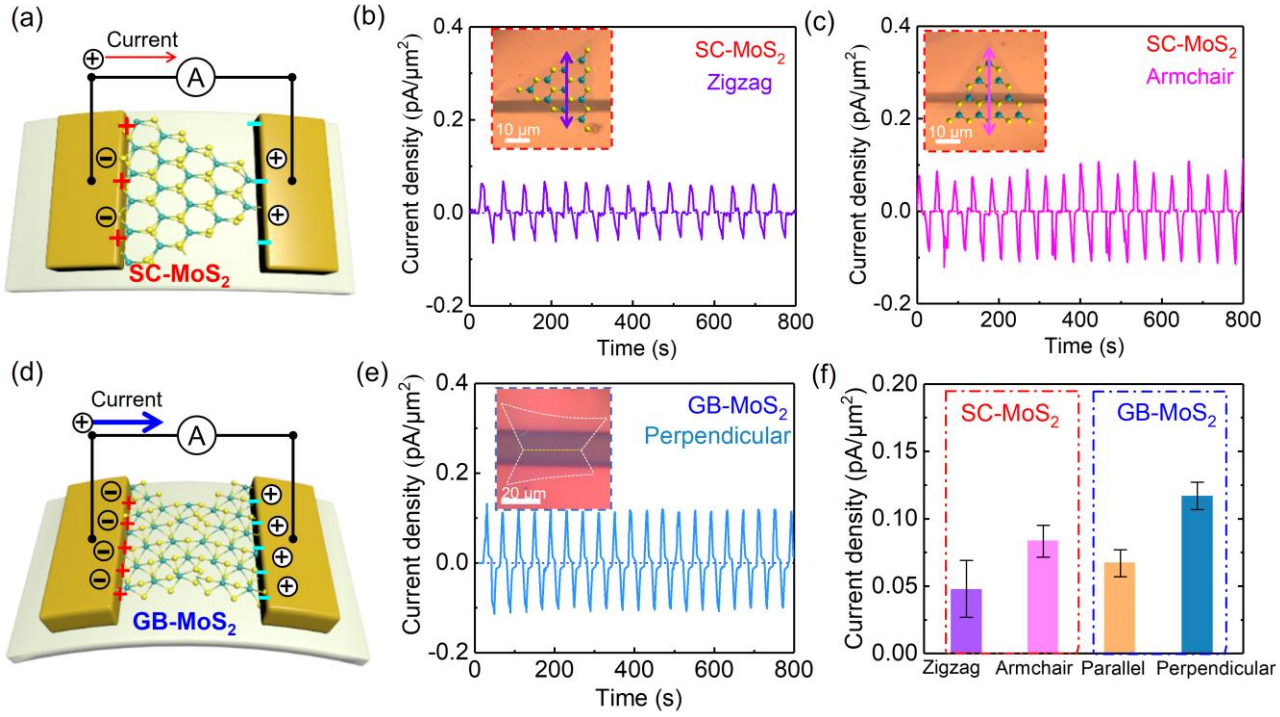

Figure 4. Piezoelectric properties measured from monolayer MoS_2 flakes. (a) The schematic of a piezoelectric device based on an SC-MoS_2 flake. The optical image of the flexible MoS_2 piezoelectric device. (b,c) Current outputs recorded from the SC-MoS_2 piezoelectric devices along the zigzag and armchair orientations under a period tensile strain of 0.56%. (d) The GB-MoS_2 flake based device. (e) Current outputs obtained from the GB-MoS_2 piezoelectric device perpendicular to the grain boundary direction under a period tensile strain of 0.56%. (f) The statistics of the current density of different monolayer MoS_2 based piezoelectric devices under the same experimental conditions.

As previously reported, the piezoelectric output was different when it was measured along the "armchair" and "zigzag" directions of the monolayer MoS_2.[20] To investigate the dependence of piezoelectricity of monolayer MoS_2 on its atomic orientation axis, we fabricated two

kinds of devices using triangle monolayer SC-MoS_2 with different orientations and measured the current outputs (Figure S11). The output-current density results displayed in Figure 4b and 4c shows that the generated current values of devices along the "armchair" direction of monolayer MoS_2 were higher than those along the "zigzag" direction. These results are consistent with the previous resport.[20]

As for GB-MoS_2 based devices shown in Figure 4e and Figure S12a, the current density (about 0.07-0.12 pA/μm^2) are much larger than those from the monolayer MoS_2 without the GBs (0.05-0.08 pA/μm^2). This experimental result matches well with the theoretical calculation. The detail of polarization of 5-7 atom-ring in GB is illustrated in Figure S13. Figure S14 shows the current outputs of piezoelectric devices made of monolayer MoS_2 with GBs as a function of the strains. When the tensile strain is increased from 0.42% to 0.7%, the corresponding piezoelectric output current increases from 20 to 60 pA, showing an increasing piezo-outputs with tensile strain in the device of monolayer GB-MoS_2.[6] Stabilities of both types of devices (without GB and with GB) were tested and the results are shown in Figure S12a, Figure S15, and Figure S16, respectively. The energy conversion of both types of device from the piezoelectric effects was stable over time even after 3000 s. In addition, the polar switching test was also shown in Figure S17. These results clearly demonstrated the excellent piezoelectric effect of the monolayer MoS_2 with GBs.[4,6] Furthermore, we have carried out statistical analysis of electromechanical measurement results obtained from different devices as shown in Figure 4f. Based on the statistical results, we can find that the current density outputs along the "armchair" directions of the monolayer MoS_2 are higher than those along with the "zigzag" directions. More importantly, the current output results from the devices with the GBs (both the perpendicular and parallel to the GB direction) are higher than those from the SC-MoS_2 monolayer nanoflakes, indicating the indeed piezoelectricity enhancement by GBs.

Application of Butterfly-Shaped Monolayer MoS_2 in Piezotronic Devices. Generally, the pressure sensors for most applications, such as electronic-skin, healthcare monitoring, and wearable sensors, require high sensitivity, fast response speed and low-power consumption.[39] To verify that our devices can meet the stringent requirements in wearable intelligent systems and wearable healthcare applications, we fabricated a pressure sensor based on the butterfly-shaped MoS_2 with GBs by using an ultrathin (about 200 μm) PDMS film as the substrate. The device can be attached to a human's wrist demonstrating its high reliability and functionality in a tension state. Furthermore, the wrist pulses were able to be read out accurately under a normal condition, which is ~ 72 beats per minute (bpm) (Figure 5b) even without any voltage biases. This indicates that our device not only possesses a high sensitivity, but also can work with low-power consumption.[9] However, the signals are indistinct and irregular when using SC-MoS_2 monolayers due to its lower piezoelectric sensitivity (Figure S18). The more obvious and regular signals obtained from GB-MoS_2 sensor than that from SC-MoS_2 sensor indicates its greater potential for practical applications in testing pulse. In addition to healthcare applications, our piezoelectric device of GB-MoS_2 can also be used as a pressure sensor to detect the pressing forces as schematically shown in Figure 5c. The sensor showed good responses at different applied mechanical forces of 0.15N, 0.25N and 0.5N as shown in Figure 5d, along with very good signal to noise ratios. The current outputs increase with increasing forces. All these results demonstrate a high sensitivity and a greater potential for practical applications of our GB-MoS_2 pressure sensors.

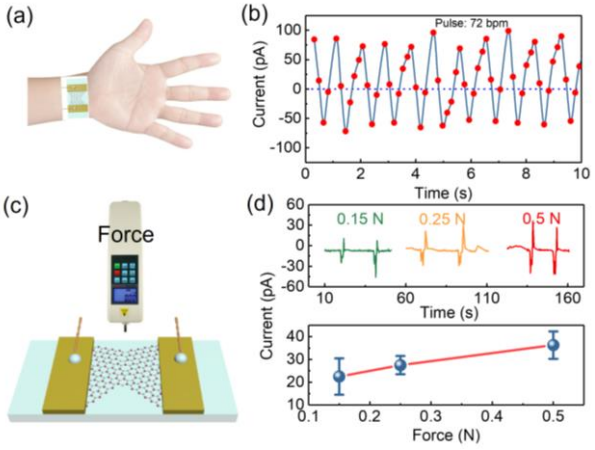

Figure 5. Practical applications of the GB-MoS_2 piezoelectric devices. a) The schematic diagram of the testing pulse. b) The corresponding current signals obtained when testing pulse. c) The schematic diagram of the mechanical sensor. d) The current outputs under different applied force and the corresponding relationship between output current peaks and applied forces.

Conclusions

In summary, we revealed the impact of GBs in monolayer MoS_2 on the piezoelectricity. Through systematical characterization of the structure of GBs in MoS_2 monolayers and theoretical verification, we found that the defects at the GBs changed the symmetry of MoS_2 crystal structures, thus producing more polarization charges under an external strain. Our experimental results showed that the piezoelectric power outputs of the GB-MoS_2 monolayers could be improved by about 50% when comparing with those from SC-MoS_2 monolayers. Our findings will help break the limit by GBs in 2D piezoelectrics for practical applications, and also make the mechanical

energy harvest more effective by using flexible 2D piezoelectric devices.

ASSOCIATED CONTENT

The Supporting Information is available free of charge on the ACS Publications website.

Experimental section and method, Additional figures S1-S18. (PDF)

AUTHOR INFORMATION

Corresponding Author

* hupa@hit.edu.cn; zh0005xi@szu.edu.cn

ORCID

Mingjin Dai: 0000-0001-6009-1715

Jia Zhang: 0000-0003-0943-7543

Yunfeng Qiu: 0000-0002-0163-4908

PingAn Hu: 0000-0003-3499-2733

Author Contributions

#These authors contributed equally.

The authors declare no competing financial interest.

ACKNOWLEDGMENT

We thank Y. Zhang, Prof. S. W. Wu for SHG characterization. This work is supported by the National Natural Science Foundation of China (NSFC, 61390502, 21373068), the Foundation for Innovative Research Groups of the National Natural Science Foundation of China (Grant No.51521003), Self-Planned Task (No. SKLRS201607B) of State Key Laboratory of Robotics and System (HIT), UK Engineering Physics and Science Research Council (EPSRC EP/P018998/1) and the Newton Mobility Grant (IE161019) through the Royal Society and NFSC.

REFERENCES

(1) Cross, E., Materials Science-Lead-Free at Last. *Nature* **2004,** *432*, 24-25.
(2) Scott, J. F., Applications of Modern Ferroelectrics. *Science* **2007,** *315*, 954-959.
(3) Sun, E. W.; Cao, W. W., Relaxor-Based Ferroelectric Single Crystals: Growth, Domain Engineering, Characterization and Applications. *Prog. Mater Sci.* **2014,** *65*, 124-210.
(4) Wang, Z. L.; Song, J. H., Piezoelectric Nanogenerators Based on Zinc Oxide Nanowire Arrays. *Science* **2006,** *312*, 242-246.
(5) Kingon, A. I.; Srinivasan, S., Lead Zirconate Titanate Thin Films Directly on Copper Electrodes for Ferroelectric, Dielectric and Piezoelectric Applications. *Nat, Mater.* **2005,** *4*, 233-237.
(6) Wu, W. Z.; Wang, L.; Li, Y. L.; Zhang, F.; Lin, L.; Niu, S. M.; Chenet, D.; Zhang, X.; Hao, Y. F.; Heinz, T. F.; Hone, J.; Wang, Z. L., Piezoelectricity of Single-Atomic-Layer MoS_2 for Energy Conversion and Piezotronics. *Nature* **2014,** *514*, 470-474.
(7) Zhu, H. Y.; Wang, Y.; Xiao, J.; Liu, M.; Xiong, S. M.; Wong, Z. J.; Ye, Z. L.; Ye, Y.; Yin, X. B.; Zhang, X., Observation of Piezoelectricity in Free-Standing Monolayer MoS_2. *Nat. Nanotechnol.* **2015,** *10*, 151-155.
(8) Hinchet, R.; Khan, U.; Falconi, C.; Kim, S. W., Piezoelectric Properties in Two-Dimensional Materials: Simulations and Experiments. *Mater. Today* **2018,** *21*, 611-630.
(9) Dai, M.; Wang, Z.; Wang, F.; Qiu, Y.; Zhang, J.; Xu, C.-Y.; Zhai, T.; Cao, W.; Fu, Y.; Jia, D.; Zhou, Y.; Hu, P.-A., Two-Dimensional van der Waals Materials with Aligned in-Plane Polarization and Large Piezoelectric Effect for Self-Powered Piezoelectric Sensors. *Nano Lett.* **2019,** *19*, 5410-5416.
(10) Bertolazzi, S.; Brivio, J.; Kis, A., Stretching and Breaking of Ultrathin MoS_2. *ACS Nano* **2011,** *5*, 9703-9709.
(11) Yang, Y. C.; Li, X.; Wen, M. R.; Hacopian, E.; Chen, W. B.; Gong, Y. J.; Zhang, J.; Li, B.; Zhou, W.; Ajayan, P. M.; Chen, Q.; Zhu, T.; Lou, J., Brittle Fracture of 2D $MoSe_2$. *Adv. Mater.* **2017,** *29*, 1604201.
(12) Feng, W.; Zheng, W.; Gao, F.; Chen, X. S.; Liu, G. B.; Hasan, T.; Cao, W. W.; Hu, P. A., Sensitive Electronic-Skin Strain Sensor Array Based on the Patterned Two-Dimensional Alpha-In_2Se_3. *Chem. Mater.* **2016,** *28*, 4278-4283.
(13) Zheng, W.; Huang, W. C.; Gao, F.; Yang, H. H.; Dai, M. J.; Liu, G. B.; Yang, B.; Zhang, J.; Fu, Y. Q.; Chen, X. S.; Qiu, Y. F.; Jia, D. C.; Zhou, Y.; Hu, P. A., Kirigami-Inspired Highly Stretchable Nanoscale Devices Using Multidimensional Deformation of Monolayer MoS_2. *Chem. Mater.* **2018**, *30*, 6063-6070.
(14) Dai, M. J.; Chen, H. Y.; Feng, R.; Feng, W.; Hu, Y. X.; Yang, H. H.; Liu, G. B.; Chen, X. S.; Zhang, J.; Xu, C. Y.; Hu, P. A., A Dual-Band Multilayer InSe Self-Powered Photodetector with High Performance Induced by Surface Plasmon Resonance and Asymmetric Schottky Junction. *ACS Nano* **2018,** *12*, 8739-8747.
(15) Zheng, W.; Feng, W.; Zhang, X.; Chen, X. S.; Liu, G. B.; Qiu, Y. F.; Hasan, T.; Tan, P. H.; Hu, P. A., Anisotropic Growth of Nonlayered CdS on MoS_2 Monolayer for Functional Vertical Heterostructures. *Adv. Funct. Mater.* **2016,** *26*, 2648-2654.
(16) Dai, M.; Chen, H.; Wang, F.; Hu, Y.; Wei, S.; Zhang, J.; Wang, Z.; Zhai, T.; Hu, P., Robust Piezo-Phototronic Effect in Multilayer γ-InSe for High-Performance Self-Powered Flexible Photodetectors. *ACS Nano* **2019,** *13*, 7291-7299.
(17) Michel, K. H.; Verberck, B., Phonon Dispersions and Piezoelectricity in Bulk and Multilayers of Hexagonal Boron Nitride. *Phys. Rev. B* **2011,** *83*, 115328.
(18) Zhang, J.; Meguid, S. A., Piezoelectricity of 2D Nanomaterials: Characterization, Properties, and Applications. *Semicond. Sci. Technol.* **2017,** *32*, 043006.
(19) Duerloo, K. A. N.; Ong, M. T.; Reed, E. J., Intrinsic Piezoelectricity in Two-Dimensional Materials. *J. Phys. Chem. Lett.* **2012,** *3*, 2871-2876.
(20) Kim, S. K.; Bhatia, R.; Kim, T. H.; Seol, D.; Kim, J. H.; Kim, H.; Seung, W.; Kim, Y.; Lee, Y. H.; Kim, S. W., Directional Dependent Piezoelectric Effect in CVD Grown Monolayer MoS_2 for Flexible Piezoelectric Nanogenerators. *Nano Energy* **2016,** *22*, 483-489.
(21) Lee, J. H.; Park, J. Y.; Cho, E. B.; Kim, T. Y.; Han, S. A.; Kim, T. H.; Liu, Y.; Kim, S. K.; Roh, C. J.; Yoon, H. J.; Ryu, H.; Seung, W.; Lee, J. S.; Lee, J.; Kim, S. W., Reliable Piezoelectricity in Bilayer WSe_2 for Piezoelectric Nanogenerators. *Adv. Mater.* **2017,** *29*, 1606667.
(22) Han, S. A.; Kim, T. H.; Kim, S. K.; Lee, K. H.; Park, H. J.; Lee,

J. H.; Kim, S. W., Point-Defect-Passivated MoS_2 Nanosheet-Based High Performance Piezoelectric Nanogenerator. *Adv. Mater.* **2018**, *30*, 1800342.
(23) Sohn, A.; Choi, S.; Han, S. A.; Kim, T. H.; Kim, J. H.; Kim, Y.; Kim, S. W., Temperature-Dependent Piezotronic Effect of MoS_2 Monolayer. *Nano Energy* **2019,** *58*, 811-816.
(24) Fei, R. X.; Li, W. B.; Li, J.; Yang, L., Giant Piezoelectricity of Monolayer Group Iv Monochalcogenides: SnSe, SnS, GeSe, and GeS. *Appl. Phys. Lett.* **2015,** *107*, 173104.
(25) Huang, P. Y.; Ruiz-Vargas, C. S.; van der Zande, A. M.; Whitney, W. S.; Levendorf, M. P.; Kevek, J. W.; Garg, S.; Alden, J. S.; Hustedt, C. J.; Zhu, Y.; Park, J.; McEuen, P. L.; Muller, D. A., Grains and Grain Boundaries in Single-Layer Graphene Atomic Patchwork Quilts. *Nature* **2011,** *469*, 389-392.
(26) Najmaei, S.; Liu, Z.; Zhou, W.; Zou, X. L.; Shi, G.; Lei, S. D.; Yakobson, B. I.; Idrobo, J. C.; Ajayan, P. M.; Lou, J., Vapour Phase Growth and Grain Boundary Structure of Molybdenum Disulphide Atomic Layers. *Nat, Mater.* **2013,** *12*, 754-759.
(27) van der Zande, A. M.; Huang, P. Y.; Chenet, D. A.; Berkelbach, T. C.; You, Y. M.; Lee, G. H.; Heinz, T. F.; Reichman, D. R.; Muller, D. A.; Hone, J. C., Grains and Grain Boundaries in Highly Crystalline Monolayer Molybdenum Disulphide. *Nat, Mater.* **2013,** *12*, 554-561.
(28) Liu, Y. Y.; Zou, X. L.; Yakobson, B. I., Dislocations and Grain Boundaries in Two-Dimensional Boron Nitride. *ACS Nano* **2012,** *6*, 7053-7058.
(29) Gibb, A. L.; Alem, N.; Chen, J. H.; Erickson, K. J.; Ciston, J.; Gautam, A.; Linck, M.; Zettl, A., Atomic Resolution Imaging of Grain Boundary Defects in Monolayer Chemical Vapor Deposition-Grown Hexagonal Boron Nitride. *J. Am. Chem. Soc.* **2013,** *135*, 6758-6761.
(30) Rasool, H. I.; Ophus, C.; Zettl, A., Atomic Defects in Two Dimensional Materials. *Adv. Mater.* **2015,** *27*, 5771-5777.
(31) Dang, K. Q.; Spearot, D. E., Effect of Point and Grain Boundary Defects on the Mechanical Behavior of Monolayer MoS_2 under Tension *via* Atomistic Simulations. *J. Appl. Phys.* **2014,** *116*, 013508.
(32) Rong, Y. M.; Sheng, Y. W.; Pacios, M.; Wang, X. C.; He, Z. Y.; Bhaskaran, H.; Warner, J. H., Electroluminescence Dynamics across Grain Boundary Regions of Monolayer Tungsten Disulfide. *ACS Nano* **2016,** *10*, 1093-1100.
(33) Hsieh, K.; Kochat, V.; Zhang, X.; Gong, Y. J.; Tiwary, C. S.; Ajayan, P. M.; Ghosh, A., Effect of Carrier Localization on Electrical Transport and Noise at Individual Grain Boundaries in Monolayer MoS_2. *Nano Lett.* **2017,** *17*, 5452-5457.
(34) Cheng, J. X.; Jiang, T.; Ji, Q. Q.; Zhang, Y.; Li, Z. M.; Shan, Y. W.; Zhang, Y. F.; Gong, X. G.; Liu, W. T.; Wu, S. W., Kinetic Nature of Grain Boundary Formation in as-Grown MoS_2 Monolayers. *Adv. Mater.* **2015,** *27*, 4069-4074.
(35) Liu, Z.; Amani, M.; Najmaei, S.; Xu, Q.; Zou, X. L.; Zhou, W.; Yu, T.; Qiu, C. Y.; Birdwell, A. G.; Crowne, F. J.; Vajtai, R.; Yakobson, B. I.; Xia, Z. H.; Dubey, M.; Ajayan, P. M.; Lou, J., Strain and Structure Heterogeneity in MoS_2 Atomic Layers Grown by Chemical Vapour Deposition. *Nat. Commun.* **2014,** *5*, 5246.
(36) Delley, B., An All-Electron Numerical-Method for Solving the Local Density Functional for Polyatomic-Molecules. *J. Chem. Phys.* **1990,** *92*, 508-517.
(37) Perdew, J. P.; Burke, K.; Ernzerhof, M., Generalized Gradient Approximation Made Simple. *Phys. Rev. Lett.* **1996,** *77*, 3865-3868.
(38) Zhang, L.; Wan, L. H.; Yu, Y. J.; Wang, B.; Xu, F. M.; Wei, Y. D.; Zhao, Y., Modulation of Electronic Structure of Armchair MoS_2 Nanoribbon. *J. Phys. Chem. C.* **2015**, *119*, 22164.
(39) Schwartz, G.; Tee, B. C. K.; Mei, J. G.; Appleton, A. L.; Kim, D. H.; Wang, H. L.; Bao, Z. N. Flexible Polymer Transistors with High Pressure Sensitivity for Application in Electronic Skin and Health Monitoring. *Nat. Commun.* **2013**, *4*, 1859.

ToC: